



## Response surface methodology approach for optimization of norfloxacin by the graphene oxide under the presence of tannic acid and its adsorption mechanism

Parnuch Hongsawat<sup>a,\*</sup>, Supakorn Bungokule<sup>a</sup>, Natnicha Boonchouy<sup>a</sup>, Panida Prarat<sup>a</sup>, Patiparn Punyalakul<sup>b,c</sup>

<sup>a</sup>Faculty of Science Energy and Environment, King Mongkut's University of Technology North Bangkok, Rayong 21120, Thailand, Tel. +6689 7760032; email: parnuch.h@sciee.kmutnb.ac.th (P. Hongsawat)

<sup>b</sup>Department of Environmental Engineering, Faculty of Engineering, Chulalongkorn University, Bangkok 10330, Thailand

<sup>c</sup>Research Unit Control of Emerging Micropollutants in Environment, Chulalongkorn University, Bangkok 10330, Thailand

Received 1 May 2020; Accepted 27 November 2020

### ABSTRACT

Graphene oxide (GO) synthesized was used as the adsorbent and had its physicochemical properties characterized by scanning electron microscope, transmission electron microscope, X-ray powder diffraction and FT-IR. These results demonstrated the complete synthesis of GO. To understand the adsorption mechanism of norfloxacin (NOR) by GO, equilibrium data were fitted to the non-linear Langmuir, Freundlich and Sips isotherm model, the data were best suited to the Sips isotherm model. The adsorption capacities of NOR by GO under the presence of tannic acid (TA) were optimized via Box–Behnken experimental design in combination with response surface methodology (RSM) approach. Independent variables including the concentration of NOR (10–80 ppm), pH (pH 4–9) and concentration of TA (2–10 ppm) were established as a conducting base for the design of 30 experiments. The results showed that the zwitterionic form of NOR had the highest adsorption capacity (pH 6–9), which suggests it might have been caused by the hydrophobic interaction. In order to clarify adsorption mechanism, the X-ray photoelectron spectroscopy analysis was applied to examine it in detail. Therefore, these results elucidate that a combination between  $\pi$ - $\pi$  electron donor–acceptor (EDA) interaction, hydrogen bonding and hydrophobic interaction was the key in the adsorption mechanism of NOR by the GO under the presence of TA.

*Keywords:* Adsorption mechanism; Norfloxacin; Graphene oxide; Response surface methodology; Tannic acid

### 1. Introduction

Norfloxacin (NOR) is one of the most commonly used fluoroquinolone antibiotics in both medical and veterinary fields. As it is overused, there are various sources of antibiotic contamination of the aquatic environment, for example, through the discharge from manufacturing facilities, factories, hospitals, municipal sewage systems and agricultural industry, through livestock manure, etc. As a result,

the detection and impact of NOR on the aquatic environment is becoming a great concern as an array of micropollutants emerges worldwide [1–4]. Due to its properties of stability and recalcitrant nature, NOR can stay in the environment for a long time. This leads to an increase of bacterial resistance to NOR in wastewater from the sources as well as a rise in concern about its harm to human health [1].

Adsorption is the promising process used in the removal of antibiotics from contaminated water and wastewater due to its simplicity, effectiveness, low cost, ease of operation

\* Corresponding author.

and capacity for scalability [5]. From the literature review, it was found that dissolved organic matter (DOM) has a reducing effect on antibiotic adsorption by carbonaceous adsorbent [4,6,7]. Tannic acid (TA) is a hydrophobic DOM that commonly presents itself in surface and ground water; it acts as the intermediate compound or competitive compound in the adsorption treatment process [8]. In our previous study, the presence of TA had a decreasing effect on the adsorption of oxytetracycline (OTC) antibiotic onto the modified GO at low concentrations whilst it could enhance the adsorption capacity of OTC at high concentrations [9]. Based on the above knowledge, TA should be taken into consideration for further development in the adsorption processes especially in the selective adsorption. Among the various kinds of adsorbents, graphene oxide (GO) is a competitive candidate for selective adsorption of NOR from the aquatic environment because of its surface that is composed of an abundance of oxygen-containing functional groups such as carboxyl (–COOH), hydroxyl (–OH), carbonyl (–C=O) and epoxy (–C–O–C–). Moreover, GO as an adsorbent is an outstanding achiever due to its physicochemical properties such as abundant pore structure, high surface area and two-dimensional graphene surface that can conduct and a strong tendency to interact with an organic compound [10].

The aim of this research is to evaluate and consider the adsorption of NOR by GO under the presence of TA, which is the major component of natural organic matter (NOM) in the aquatic environment. Hopefully, this will provide valuable guidance and become an effective method for the removal of NOR from the aquatic environment. To optimize the adsorption capacities of NOR by GO under the presence of tannic acid (TA), Box–Behnken experimental design (BBD) combining with response surface methodology (RSM) – a statistical technique that can be used to determine the optimal conditions in the variable control approaches – was applied in this research. Besides, it has an advantage of time and cost reduction. Apart from this advantage, there are also applications of the adsorption process to demonstrate the relationship among various factors in one or more responses [11–15]. To better understand the adsorption mechanism, adsorption isotherm and X-ray photoelectron spectroscopy (XPS) were analyzed to clarify it in detail.

## 2. Method

### 2.1. Materials and chemicals

The analytics of all higher grades of all chemicals and reagents were carried out in this work while analytical solvents used were of HPLC grade. Activated carbon along with the graphite powder was supplied by Sigma-Aldrich (Missouri, United States). Hydrogen peroxide solution (H<sub>2</sub>O<sub>2</sub>, 30%), hydrochloric acid (HCl 37%), sulfuric acid (H<sub>2</sub>SO<sub>4</sub>, 96%) and phosphoric acid (H<sub>3</sub>PO<sub>4</sub>, 96%), were kindly provided by Carlo Erba (Barcelona, Spain). Potassium permanganate (KMnO<sub>4</sub>), di-potassium hydrogen orthophosphate (K<sub>2</sub>HPO<sub>4</sub>, 99%), and potassium dihydrogen orthophosphate (KH<sub>2</sub>PO<sub>4</sub>, 99%) were purchased from Ajax Finechem (New South Wales, Australia). Acetonitrile (C<sub>2</sub>H<sub>3</sub>N) was obtained from RCI Labscan Limited (Bangkok, Thailand). Distilled water was utilized throughout the

experiments for the preparation of solutions and cleaning of glass water. Norfloxacin (NOR, 99 wt.%) and tannic acid (TA, 70 wt.%) were supplied by Sigma-Aldrich (Missouri, United States). The chemical structure and physicochemical properties of NOR and TA are presented in Table 1.

### 2.2. Synthesis of graphene oxide (GO)

Graphene oxide (GO) was synthesized via oxidation of natural graphite according to the modified Hummer's method. First, graphite powder was added to concentrated sulfuric acid (120 mL) with continuous stirring while the temperature was kept at 0°C. Next, potassium permanganate (15 g) was gradually added at the same temperature. After the addition, the mixture was heated to 35°C for 2 h. Following that, distilled water (230 mL) was slowly added to the stirring solution while the reaction temperature was kept at not more than 20°C for 2 h. Then, distilled water (700 mL) and hydrogen peroxide (20 mL) were added, which turned the color of the mixture to a brownish-yellow at this step. The formed GO was then centrifuged (3,500 rpm for 10 min) and washed three times with distilled water; the mixture was subsequently subjected to the filtration and oven drying at 60°C [18].

### 2.3. Characterization of adsorbents

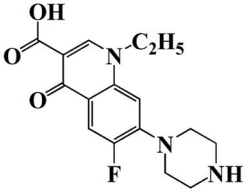
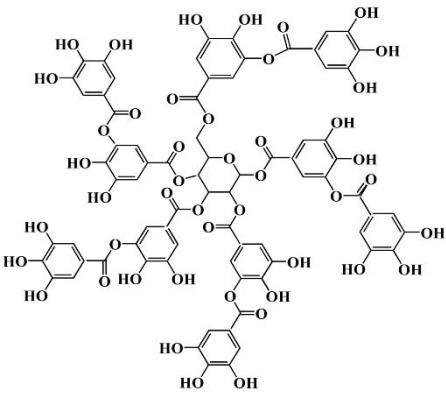
Various techniques were used to analyze the physicochemical properties of adsorbents. Morphology was carried out by a JEOL model JSM 6400 scanning electron microscope (SEM) and a JEOL model JEM 2100 transmission electron microscope (TEM). While the crystalline structure was examined by X-ray powder diffraction (XRD, Bruker AXS D8 diffractometer) using Cu-K $\alpha$  radiations. Fourier transform infrared spectrophotometry (FT-IR, PerkinElmer Spectrum One, USA) was utilized to analyze the surface functional group. The pH of the point of zero charge (pH<sub>pzc</sub>) of the adsorbents was determined according to the following procedure [19]: in each of the 10 beakers, 20 mL of NaCl (0.01 M) was placed. The pH of these solutions was adjusted by adding NaOH (0.1 M) or HCl (0.1 M) to prepare solutions with initial pH values varying between 1 and 11. After working out the initial pH<sub>i</sub>, 20 mg of the adsorbent was added to each solution and stirred for 24 h at room temperature; upon completion, the final pH<sub>f</sub> was measured to plot the pH<sub>f</sub> vs. pH<sub>i</sub> curve. The pH<sub>pzc</sub> was determined at pH<sub>f</sub> = pH<sub>i</sub>.

### 2.4. Adsorption studies

The batch adsorption experiment was carried out in a 125 mL Erlenmeyer flask containing 0.5 g L<sup>-1</sup> of the adsorbent. Buffer solution's pH and ionic strength were controlled using a 10 mM phosphate buffer. The required pH was adjusted using HCl and NaOH solutions. Experimental samples were shaken (200 rpm) at room temperature (30°C), following that they were filtered by nylon membrane (pore size 0.45  $\mu$ m). Finally, the adsorption capacity at equilibrium ( $q_e$ ) was calculated according to Eq. (1):

$$q_e = \frac{(C_0 - C_e)V}{m} \quad (1)$$

Table 1  
Chemical structure and physicochemical properties of the NOR and TA

Chemical	Chemical structure	Molecular weight (g mol <sup>-1</sup> )	pK <sub>a</sub>
Norfloracin (NOR, C <sub>16</sub> H <sub>18</sub> FN <sub>3</sub> O <sub>3</sub> )		319.30	pK <sub>a1</sub> = 6.22 <sup>a</sup> pK <sub>a2</sub> = 8.51
Tannic acid (TA, C <sub>76</sub> H <sub>52</sub> O <sub>46</sub> )		1,701.20	pK <sub>a</sub> = 10.00 <sup>b</sup>

<sup>a</sup>[16]; <sup>b</sup>[17]

where  $C_0$  (mg L<sup>-1</sup>) is the initial concentration of the NOR solution and  $C_e$  (mg L<sup>-1</sup>) is the equilibrium concentration of the NOR solution.  $V$  (L) is the volume of solution, and  $m$  (g) is the weight of adsorbent used.

#### 2.4.1. Adsorption isotherm models

To determine the adsorption isotherms, GO was conducted using phosphate buffer at pH level 5.0, 7.0, and 9.0, whilst also varying the initial concentration of NOR from 5 to 120 mg L<sup>-1</sup>. To understand the adsorption mechanism of NOR onto GO, the adsorption equilibrium isotherm data experimentally acquired were employed to the three nonlinear adsorption isotherm models of Langmuir, Freundlich and Sips as expressed in Eqs. (2)–(4).

$$q_e = \frac{q_m b C_e}{1 + b C_e} \quad (2)$$

$$q_e = K_F C_e^{1/n} \quad (3)$$

$$q_e = \frac{q_m b C_e^{1/n}}{1 + b C_e^{1/n}} \quad (4)$$

where  $q_m$  is the maximum adsorption capacity (mg g<sup>-1</sup>) and  $b$  is a Langmuir constant related to the energy of adsorption and affinity of the sorbent.  $K_F$  and  $n$  are Freundlich characteristics of the system, this indicates the adsorption affinity.

The model fitting was carried out using the solver add-in function of Microsoft Excel [20]. Fitting the degree of the isotherm models was evaluated by the correlation coefficient ( $R^2$ ) and nonlinear Chi square, which can be defined as follows:

$$R^2 = \frac{(q_{e,meas} - \overline{q_{e,calc}})^2}{\sum (q_{e,meas} - \overline{q_{e,calc}})^2 + (q_{e,meas} - q_{e,calc})^2} \quad (5)$$

$$\text{Non-linear chi square} = \sum_{i=1}^p \frac{(q_{e,calc} - q_{e,meas})^2}{q_{e,meas}} \quad (6)$$

where  $q_{e,calc}$  and  $q_{e,meas}$  are calculated and measured, adsorbate concentration at equilibrium (mg g<sup>-1</sup>),  $p$  is the number of the data point.

#### 2.4.2. Box-Behnken experimental design and optimization by RSM

To optimize the adsorption capacity of NOR onto carbonaceous adsorbents with different pH under the presence of TA, BBD under RSM via Minitab 17 was applied to this work. The dependent variable value was the adsorption capacity of each adsorbent. For the optimization of adsorption capacity of antibiotics, the preliminary single-factor study on the effect of adsorbent dosage and effect of solution pH on the removal of NOR by GO has been determined with the range of 0.50–0.80 g/L and 2.0–11.0, respectively.

The result showed that the adsorption capacity of NOR onto GO and PAC decreased when the adsorbent dosage increased as shown in Fig. S1. While a significant increase of NOR adsorption was observed when pH increased from 3.0 to 5.0, the adsorbed amounts decreased at increasing pH (Fig. S2). Therefore, we designed this experiment over a pH range 4.0–9.0 with 0.5 g/L adsorbent dosage for the suitable optimized response surface. Furthermore, the independent variables were selected to be concentration of NOR, pH, and TA that were in the ranges of 10–80 ppm, 4–9, and 2–10 ppm, respectively. Each independent variable was coded with three levels between –1 and +1. The factors with their variation levels are presented in Table 2.

The data for each set of experiments were fitted to the following quadratic polynomial as presented in Eq. (7):

$$Y = \beta_0 + \sum_{i=1}^3 \beta_i x_i + \sum_{i=1}^3 \beta_{ii} x_i^2 + \sum_{i=1}^3 \sum_{j=1}^2 \beta_{ij} x_i x_j \quad (7)$$

In order to elucidate the adsorption mechanism, XPS (PHI 5000 VersaProbe, UIVAC, Japan) was carried out with a spectrometer featuring a resolution of 0.5 eV. While a peak fitting procedure was used based on a least-squares method (software Casa XPS).

### 2.5. Analytical methods

The concentration of NOR and TA was determined using high-performance liquid chromatography (HPLC, Agilent Technology LC 1260, California, United States) in conjunction with a UV detector at 277 nm equipped with a reverse-phase C18 column (Nucleodur Eclipse Plus size 5 mm, 4.6 × 250 nm). The mobile phase was set at 80:20 (v:v) of 0.1 mM phosphoric acid solution and acetonitrile, with a flow rate of 1.5 mL min<sup>-1</sup>, while the retention time of NOR and TA was 2.32 and 1.34 min, respectively.

## 3. Results and discussion

### 3.1. Characterization of adsorbent

Morphology of synthesized GO was carefully investigated using TEM and SEM images as shown in Figs. 1a and b, respectively. The multiple sheets appeared darker in comparison with the single sheet, it looked like the smooth surface also incorporated wrinkle-like carbon sheets as shown in Fig. 1a. While the 2D nanosheet morphologies with wrinkles and folded texture that were produced by

exfoliation of graphite oxide appeared in SEM image as shown in Fig. 1b [21].

In order to confirm the physicochemical properties of synthesized GO, XRD and FT-IR were carried out. Fig. 1c shows the XRD pattern, which reveals a peak centered at  $2\theta = 12.65$  with an interlayer spacing of 6.99. That correlates to the degree of oxidation [18]. While the occurrence of well-ordered graphene can be seen due to the absence of graphite peak (002 planes at  $2\theta = 26$ ) [18,22]. Fig. 1d presents FT-IR spectra that indicate the surface functional group. The spectrum of synthesized GO revealed a broad peak of around 3,300–3,400 cm<sup>-1</sup> and 1,618 cm<sup>-1</sup> caused by O–H stretching and bending vibrations of the hydroxyl groups [23]. While C–O stretching of carbonyl and the carboxylic group appeared at 1,053; 1,380, and 1,719 cm<sup>-1</sup> [22,24]. Moreover, the peak associated with epoxide (C–O–C) and C=O contribution was measured to be at 858 and 1,440 cm<sup>-1</sup>, respectively [24], these results indicate a successful synthesis of GO as an adsorbent.

To compare the NOR's adsorption behavior with the commercial one, powder activated carbon (PAC) was chosen for evaluation of the physicochemical properties that revealed strong band at 1,395 and 1,595 cm<sup>-1</sup> corresponding to –OH vibration and C=O stretching vibrations, which indicate the existence of carboxylate groups (–COOH) on the adsorbent surface [25].

### 3.2. Adsorption isotherm

The adsorption isotherm studies are carried out to evaluate the natural adsorption mechanism of NOR onto GO at different pH ranges (pH 5, 7 and 9). First two nonlinear Langmuir and Freundlich isotherm models were applied with the data obtained from the equilibrium isotherm experiment. The Langmuir isotherm model refers to monolayer adsorption onto the surface (the adsorbed layer is one molecule in thickness) and homogeneous adsorption (all sites possess an equal affinity for the adsorbate). While the Freundlich isotherm model is widely referred to a multi-layered adsorption with a non-uniform distribution of adsorption and affinities over the heterogeneous surface [26]. However, all of the experimental data were well fitted with nonlinear Sips isotherm that was a combination of Langmuir and Freundlich isotherm models as which can be found in Fig. 2a.

In comparison with the fitting degree of these isotherm models, it can be evaluated that by using the correlation coefficient ( $R^2$ ) and the nonlinear Chi square, from the calculated values of these isotherm models as given in Table 3, it can be seen that the correlation coefficient ( $R^2$ ) values (close to unity) and Chi square values (low value) are best fitted with the Sips isotherm model [27]. Therefore implying that the adsorption of NOR onto GO effectively reduces the Freundlich isotherm model at a low concentration of NOR, while at high concentrations it will reveal a monolayer adsorption capacity characteristic found in the Langmuir isotherm model [26,28].

According to the derived isotherm parameters as listed in Table 3, the maximum adsorption capacity ( $q_m$ ) of NOR onto GO via the Langmuir isotherm was higher than the experimental one. While the maximum adsorption capacity

Table 2  
Independent variable levels and codified values of the Box–Behnken experimental design

Factors	Coded factor	Levels		
		–1	0	1
Initial concentration of NOR (mg L <sup>-1</sup> )	$X_1$	10	45	80
pH	$X_2$	4	6.5	9
Initial concentration of TA (mg L <sup>-1</sup> )	$X_3$	2	6	10

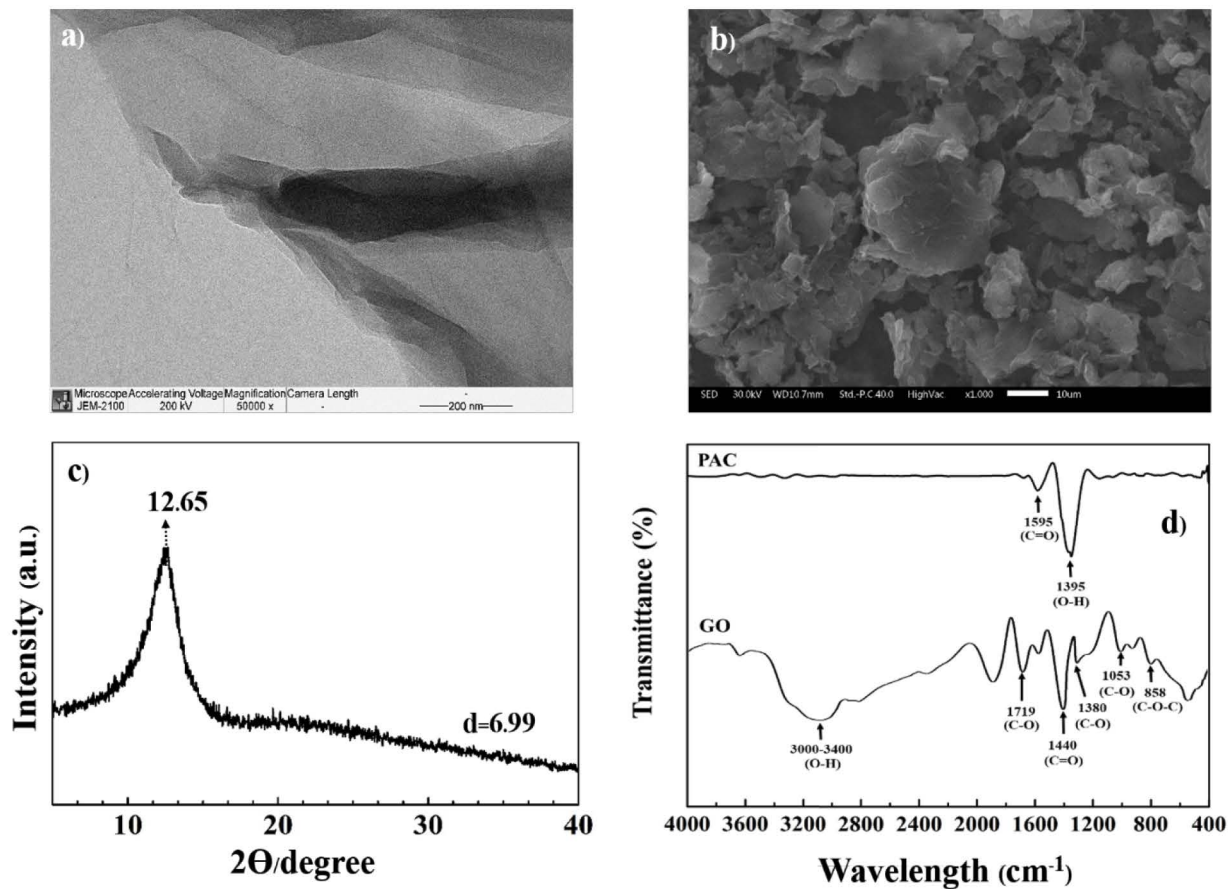


Fig. 1. Characteristics of synthesized GO: (a) TEM, (b) SEM, (c) XRD, and (d) FT-IR (FT-IR spectra of synthesized GO and commercial PAC).

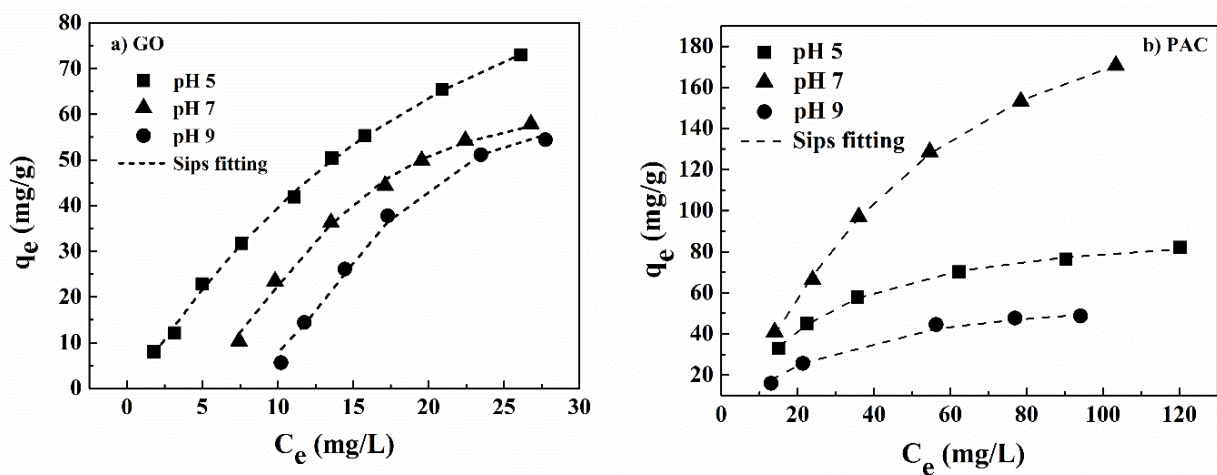


Fig. 2. Fitting curves of the Sips isotherm model of NOR adsorption onto (a) GO and (b) PAC at different pH levels: pH 5, 7 and 9.

of NOR onto GO by Sips isotherm model was more consistent with the experimental value that was found to be  $124.18 \text{ mg g}^{-1}$  at pH 5, higher than pH 7 and 9. Therefore, the Sips model produced the best fitting isotherm parameters value for all cases studies whilst also providing the lowest error values. Also, the Freundlich constant  $1/n$  was smaller

than 1; this indicated the favorable adsorption of NOR onto GO as the chemisorption.

Moreover, these results supported the heterogeneous distribution of various functional GO surfaces such as carboxylic ( $-\text{COOH}$ ), hydroxyl ( $-\text{OH}$ ) and epoxy group. On the other hand, the  $1/n$  value in Sips isotherm model was higher

Table 3  
Adsorption isotherm constants and statistical comparison values

Isotherm	pH		
	5	7	9
<b>Langmuir</b>			
$q_m$ (mg g <sup>-1</sup> )	163.54	470.57	1,554.44
$B$	0.0316	0.0056	0.0012
$R^2$	0.9975	0.9426	0.9361
Chi square	0.74	8.13	42.16
<b>Freundlich</b>			
$K_f$ (mg g <sup>-1</sup> )	7.10	2.69	0.54
$1/n$	0.7288	0.9579	1.4126
$R^2$	0.9883	0.9317	0.9053
Chi square	2.91	7.62	17.13
<b>Sips</b>			
$q_m$ (mg g <sup>-1</sup> )	124.18	63.70	64.02
$B$	0.0326	0.0008	0.0001
$1/n$	1.1579	2.8602	3.5526
$R^2$	0.9985	0.9957	0.9886
Chi square	0.34	0.45	4.19

than 1 and this might be identified as a cooperative uptake NOR molecule onto GO [26,29].

As shown in Fig. 2b, the adsorption isotherm of NOR onto PAC exhibited the higher adsorption capacity than GO. Meanwhile, it fitted well with nonlinear Sips model at every pH condition as same as the adsorption of NOR onto GO. Furthermore, the isotherm parameters obtained for NOR adsorption onto PAC from the nonlinear Sips model (Table S2) revealed the highest maximum adsorption capacity ( $q_m$ ) of NOR onto PAC at pH 7 (229.21 mg/g). However, the maximum adsorption capacity of NOR onto GO was found to be better than PAC at pH 5 (92.47 mg/g). These results suggest the different key adsorption behaviors of the uptake of NOR onto the two carbonaceous adsorbents. To enhance the adsorption efficiencies of NOR onto GO, the adsorption mechanism should be investigated for further removal of NOR under the presence of coexisting natural organic matter.

In comparison with other adsorbents used for the removal of NOR from the previous report, the equilibrium adsorption capacity ( $q_e$ , mg/g) at the similar adsorption condition was considered. Even though the adsorption capacity of GO in this study is not as high as some other adsorbents such as nitrogen modified reduced graphene oxide (110 mg/g), nitrogen modified reduced graphene oxide incorporated with magnetic (127 mg/g), powder activated carbon (114 mg/g) and granular activated carbon (59 mg/g), it could perform better than magnetic graphene oxide (30 mg/g), Magnetic molecularly imprinted polymer (14 mg/g) and magnetic molecular imprinted chitosan/ $\gamma$ -Fe<sub>2</sub>O<sub>3</sub> (8 mg/g) [30–33]. Therefore, the synthesized GO in this research could be one of the adsorbents applicable to the removal of NOR in adsorption process. However, further

research should be done to investigate the functionalized surface GO that might increase the adsorption capacity.

### 3.3. Model results and analysis

To optimize adsorption capacity and selectivity of NOR onto carbonaceous adsorbents with different pH under the presence of TA, the experimental adsorption capacity ( $q_{exp}$ ) was obtained and generated to predict adsorption capacity using the quadratic model ( $q_{mod}$ ) through the BBD. According to Table 4, a quadratic polynomial regression modeling in coded form was derived. While, the final equations for the NOR's adsorption on GO and PAC can be described in Eqs. (8) and (9), respectively:

$$q_{mod,GO} = 124.30 + 115.30X_1 + 24.9X_2 + 18.0X_1X_2 + 30.4X_3^2 \quad (8)$$

$$q_{mod,PAC} = -32.6 + 6.5X_1 - 2.19X_2 - 3.82X_3 + 0.512X_2X_3 - 0.0488X_1^2 \quad (9)$$

The reliability of both the quadratic models was evaluated by the conventional statistical metrics ( $R^2$ , adjusted  $R^2$ , predicted  $R^2$ , lack of fit, and  $F$ -value and  $P$ -value). The significance of each coefficient was determined by the  $P$ -value. If the  $P$ -value was lower than 0.05 (at 95% confidence level), the coefficient is then considered for a final model. In general, the regression coefficients ( $R^2$ , adjusted  $R^2$ , predicted  $R^2$ ) should be close to each other [34,35]. These results represent the degree of closeness to each other at around 60%–80%, which was acceptable for the description of the optimized adsorption efficiency by BBD ( $R^2 > 60\%$ ) [36] while the  $P$ -values of lack of fit for both of the GO and PAC show higher than 0.05, and the  $F$ -values lower than 0.05 indicate insignificance. Thus, the model was reliable for the NOR's adsorption capacities in these conditions.

### 3.4. Interpretation of surface and contour plots for adsorption mechanism

Three-dimensional (3D) response surfaces and contour lines showing the interaction effects of an independent parameter on the NOR adsorption capacity via GO and PAC obtained from BBD experiments are represented in Fig. 3 and Table 5. Even though the conditions were the same, increasing the amount of TA did not affect NOR's adsorption capacity. This result indicated that the concentration of TA was not significant to affect their adsorption capacities as demonstrated by the 3D response surface (Fig. 3) and  $P$ -value  $> 0.05$  (Table 4). On the other hand, the peak adsorption capacity of NOR under the presence of TA via both adsorbents was reached when the pH was in the range between 6 and 9 (as shown in Fig. 3).

What can also be seen when comparing these carbonaceous adsorbents is that the surface area and pore volume of PAC were higher than that of GO (as shown in Table S1). It was shown that GO had a higher adsorption capacity of NOR under the presence of TA than PAC.

The level of pH had a direct effect on the adsorption behavior of NOR by GO. The pH value contributed to the



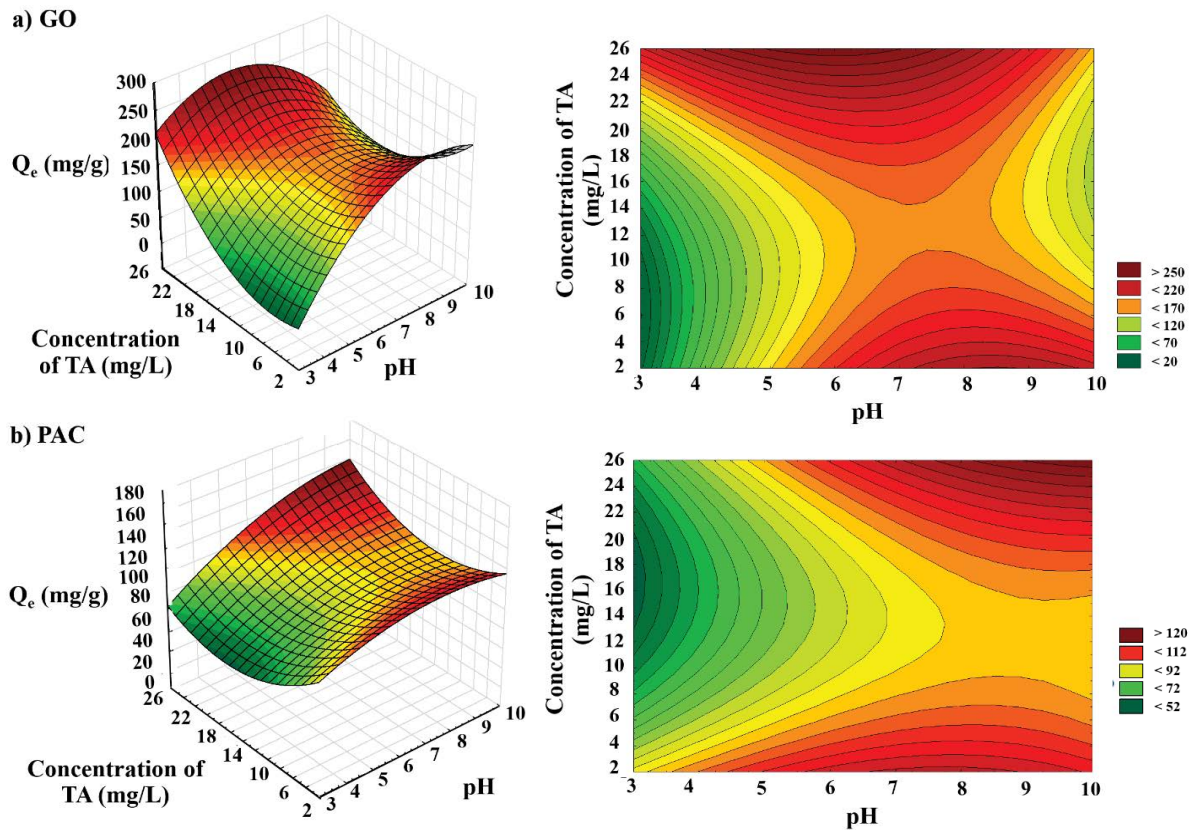


Fig. 3. Three-dimensional model (3D) of response surfaces and contour lines showing the interaction effects between pH and concentration of TA on the NOR adsorption capacity via GO (a) and PAC (b) as the adsorbents.

Table 4  
Analysis of variance for adsorption of the NOR by both carbonaceous adsorbents

Source	GO			PAC		
	<i>F</i> -value	<i>P</i> -value	Remarks	<i>F</i> -value	<i>P</i> -value	Remarks
Model	16.95	0.000	Significant	11.41	0.000	Significant
Block	1.57	0.222		5.48	0.029	Significant
Linear	41.28	0.000	Significant	16.62	0.000	Significant
$X_1$ : Initial concentration of NOR	78.73	0.000	Significant	48.76	0.000	Significant
$X_2$ : pH	3.90	0.060		1.47	0.238	
$X_3$ : Initial concentration of TA	–	–		0.26	0.615	
Square	2.20	0.151		12.67	0.002	Significant
$X_3X_3$	2.20	0.151		12.67	0.002	Significant
2-way interaction	1.06	0.315		0.95	0.341	
$X_1X_2$	1.06	0.315		0.95	0.341	
Lack of fit	2.32	0.102	Insignificant	1.75	0.202	Insignificant
	$R^2 = 77.94\%$	$R^2(\text{adj}) = 73.34\%$	$R^2(\text{pred}) = 61.26\%$	$R^2 = 76.09\%$	$R^2(\text{adj}) = 69.06\%$	$R^2(\text{pred}) = 61.26\%$

surface charge of the adsorbent as well as it is the NOR's chemical structure, with electrostatic interaction playing one of the most important roles. To expand on the surface charge of adsorbents, the value of point zero charge ( $\text{pH}_{\text{pzc}}$ )

was determined. Fig. 4a represents the variation of final pH ( $\text{pH}_f$ ) vs. initial pH ( $\text{pH}_i$ ) for both carbonaceous adsorbents. This result indicated the  $\text{pH}_{\text{pzc}}$  of GO and PAC to be at 3.10 and 7.10, respectively. When the pH had a higher value,

Table 5  
Experimental Box–Behnken design matrix, measurements ( $q_{\text{exp}}$ )

Run	Factors			PAC	GO
	Initial concentration of NOR ( $\text{mg L}^{-1}$ ) $X_1$	pH $X_2$	Initial concentration of TA ( $\text{mg L}^{-1}$ ) $X_3$	$q_{\text{exp}}$ ( $\text{mg g}^{-1}$ )	$q_{\text{exp}}$ ( $\text{mg g}^{-1}$ )
1	80	6.5	3	89.28	269.41
2	80	6.5	25	50.76	19.65
3	10	9	14	5.77	21.70
4	45	9	25	86.20	173.12
5	80	9	14	138.13	167.70
6	10	4	14	50.76	14.48
7	45	6.5	14	68.67	158.10
8	45	9	3	94.32	266.73
9	45	6.5	14	97.58	165.44
10	45	4	25	72.10	130.71
11	80	4	14	7.77	36.85
12	45	4	3	89.69	153.11
13	45	6.5	14	52.55	277.55
14	10	6.5	3	70.82	136.13
15	10	6.5	25	76.07	131.83
16	45	9	3	4.77	24.07
17	80	4	14	26.15	289.81
18	45	4	25	62.91	148.87
19	10	4	14	17.04	286.70
20	10	6.5	3	12.35	287.08
21	80	9	14	85.98	170.55
22	80	6.5	3	12.33	290.05
23	45	6.5	14	12.12	155.52
24	45	4	3	3.77	36.71
25	10	9	14	16.14	39.97
26	4	9	25	84.68	176.22
27	45	9	25	11.74	39.48
28	10	9	3	69.45	278.68
29	45	6.5	14	12.03	41.28
30	10	6.5	25	80.11	128.43

the adsorbent's surface became negatively charged. On the other hand, when the pH value was below  $\text{pH}_{\text{pzc}}$ , the surface became positively charged. Whereas, the chemical structure of NOR has two proton-binding sites corresponding to the value of acid dissociation constant ( $\text{pK}_a$ ) though carboxylic ( $\text{pK}_{a1} = 6.22$ ) and piperazinyl nitrogen group ( $\text{pK}_{a2} = 8.51$ ). When pH value is lower than  $\text{pK}_{a1}$ , the protonation of piperazinyl nitrogen occurred, so mainly NOR's structure exists in the cationic form ( $\text{NOR}^+$ ). At a higher pH value than  $\text{pK}_{a1}$  and less than  $\text{pK}_{a2}$ , deprotonation of carboxylic group results in a zwitterionic form ( $\text{NOR}^{\pm}$ ) of the solution. As a consequence, the amount of anionic form ( $\text{NOR}^-$ ) increased due to the deprotonation state of both sites. Besides this, three species of NOR corresponding to different pH values are shown in Fig. 4b.

With the presence of TA at 10 ppm; which is usually a typical concentration of NOM in drinking water [37], the highest adsorption capacity was reached at the pH range

of 6 to 9 for both adsorbents as the contour plot shown in Fig. 3. In this condition, the zwitterionic ( $\text{NOR}^{\pm}$ ) or neutral form remained as a dominant one where the amount of adsorbed NOR increased with the increase of zwitterionic form ( $\text{NOR}^{\pm}$ ), which might have been caused by hydrophobic interaction [38]. At a  $\text{pH} > 9$ , a steady decrease in the absorbing capacity was observed. That was the result of repulsion between the anionic form of NOR and the negatively charged adsorbent surface. Even when they were oppositely charged ( $3 < \text{pH} < 6$ ), the dominance of NOR and the surface charge of GO revealed as cationic form ( $\text{NOR}^+$ ) and negatively charged, the adsorption capacity was still lower. It is appropriate to reason that this was happening because of the lower hydrophobic form of the cationic form ( $\text{NOR}^+$ ) and anionic form ( $\text{NOR}^-$ ) at each pH range. As it is well known,  $\pi$ - $\pi$  EDA effect or  $\pi$ - $\pi$  EDA interaction between NOR molecules and aromatic ring of GO can occur in the adsorption mechanism



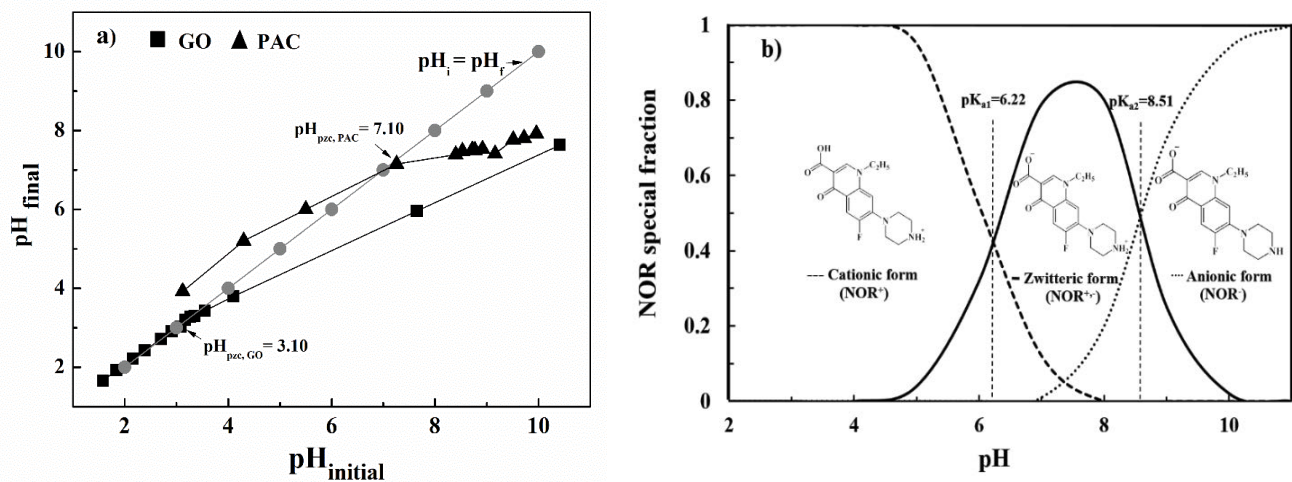


Fig. 4. (a) Surface charge of adsorbents and (b) the distribution coefficient of NOR base on their  $pH_{pzc}$  and  $pK_a$ , respectively.

[33,38–42]. Therefore, non-electrostatic interaction such as  $\pi$ - $\pi$  EDA interaction, hydrogen bonding, and hydrophobic interaction could have been involved here rather than the electrostatic interaction [23]. In contrast with some of the previous reports which looked at the adsorption of antibiotic compounds including NOR by the graphene oxide, it was found to involve electrostatic interaction in the mechanism [40,43]. It is also worth mentioning that the adsorption behavior of NOR under the presence of NOM, where NOM's competitive adsorption greatly decreased the adsorption of NOR by the adsorbent's surface [4].

### 3.5. Adsorption mechanism

In order to clarify and elaborate on the adsorption mechanism, XPS was applied to evaluate functional groups and their percentages of adsorbent surface. Fig. 5 and Table 6 demonstrate the comparison between the absorption of NOR before and after by both GO and PAC. The C1s and O1s spectra are deconvoluted and fitted to the literature [44,45].

According to C1s spectra, all of the conditions have three distinct Gaussian peaks of binding energy at ~285, 286, 288 eV could be observed, which correspond to the C=C/C–C/C–H, C–OH/epoxy, and C=O functional groups, respectively. While the adsorption of NOR by the GO presented the new peak of binding energy at 292.50 eV which suggests that the  $\pi$ - $\pi$ \* shake-up satellite during the interaction. Furthermore, the percentage component, which was calculated from deconvoluted peaks indicated that after the adsorption of NOR by GO it had relatively higher C–OH/epoxy (43.62%) and C–O (12.26%) functionalities while the lower C=O/C–C/C–H (42.09%) was observed. In the case of adsorption of NOR by PAC, all of the detected functionalities were lower than the expected C–OH/epoxy functionalities. These results implying the functional group of GO surface (C–OH and epoxy group) had participated in the adsorption of NOR.

As for deconvolution of the O1s peak, two original peaks with the binding energies (BE) at ~532 and 530 eV remained after the NOR adsorption, which was assigned to –OH and

Table 6  
XPS data of GO and PAC before and after adsorption of NOR

Components	GO		GO–NOR <sup>a</sup>		PAC		PAC–NOR <sup>a</sup>	
	BE (eV)	Area %	BE (eV)	Area %	BE (eV)	Area %	BE (eV)	Area %
C1s								
C=O/C–C/C–H	284.85	56.73	284.45	42.09	284.63	48.20	284.60	52.59
C–OH/epoxy	286.99	33.08	285.48	43.62	285.83	19.70	285.79	21.87
C=O	288.85	10.19	288.61	12.26	289.53	32.10	288.89	25.54
$\pi$ - $\pi$ shake-up satellite			292.50	2.03				
O1s								
–OH	532.84	61.42	532.91	73.72	532.47	47.66	532.90	52.88
C–O–C	530.80	38.58	531.12	21.34	531.01	21.23	531.25	29.35
			536.31	4.95	534.41	31.11	535.35	17.76

<sup>a</sup>After NOR's adsorption.

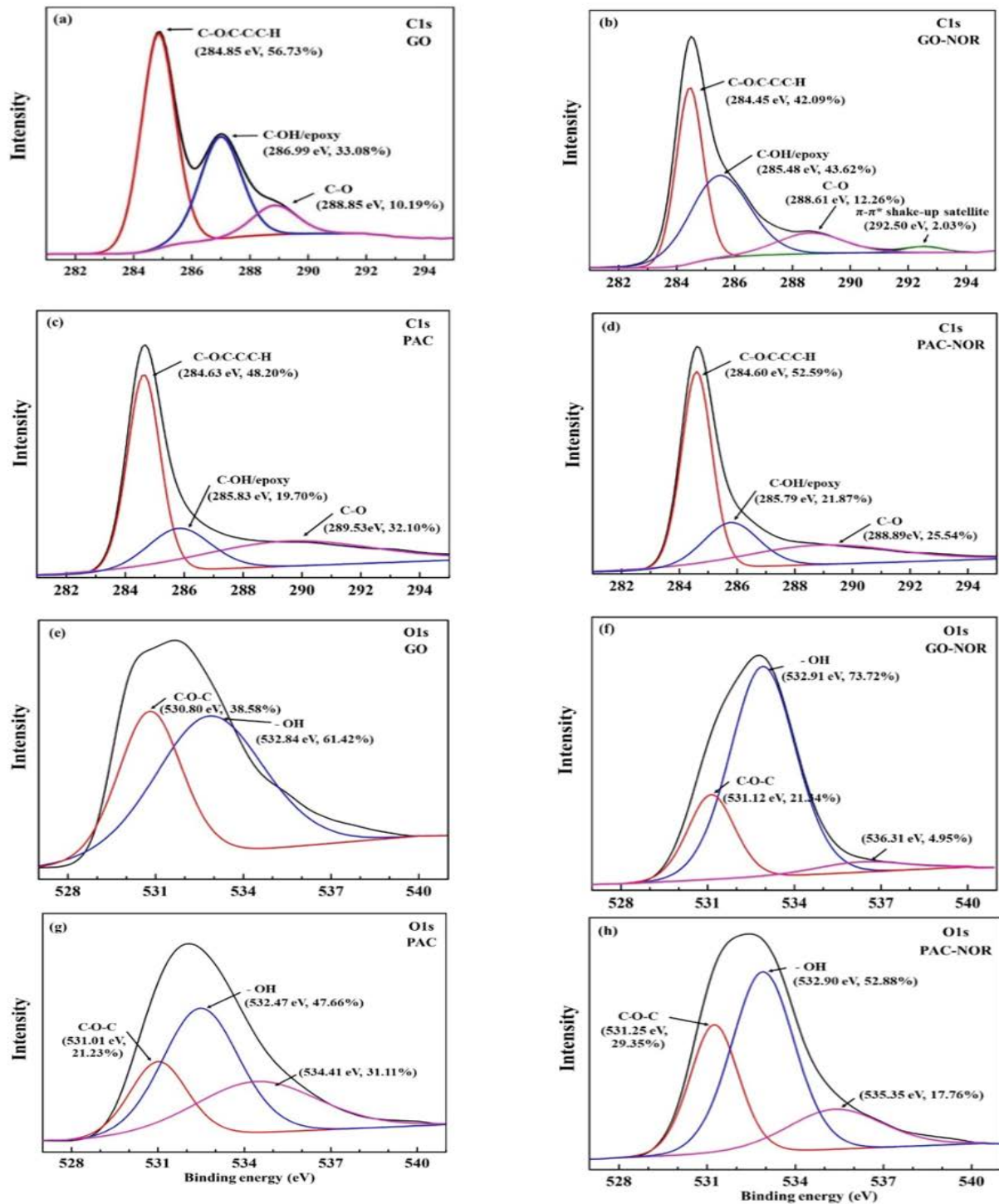


Fig. 5. XPS spectrum of carbon and oxygen before and after NOR adsorption by GO and PAC: C1s and O1s of GO (a, e) and PAC (c, g) and C1s and O1s of GO (b, f) and PAC (d, h) after NOR's adsorption.

C–O–C or C=O, respectively. During the adsorption of NOR by GO, a new peak at 536.31 eV was found in the O1s spectrum, which might have been caused by the formation of O–H...N or O–H...O complexes between GO and NOR [45]. As for results in C1s and O1s, the functional

groups of the adsorbents may have been directly involved in the adsorption interaction with NOR. While the formation of hydrogen bonds between the functional group of GO and NOR would be responsible for the NOR adsorption interaction.

Moving to the adsorption by graphene, GO and modified GO, the literature review report that  $\pi$ - $\pi$  EDA interaction, hydrogen interaction, electrostatic interaction and hydrophobic interaction have occurred as the key adsorption interactions [33,39]. When focusing on the adsorption of antibiotic by the GO,  $\pi$ - $\pi$  EDA interaction, the interaction between antibiotic molecules and electron in graphene aromatic ring was mostly presented as the dominant adsorption and assistant adsorption including hydrogen bonding and electrostatic interaction between antibiotic molecule and functional group/ physicochemical properties of GO [46–48]. In addition to hydrophobic interaction, there were also reports of the combined interactions along with other interactions [40]. For example, Zhang et al. [4] have reported on the adsorption of NOR by GO under the presence of NOM where the main interactions were an electrostatic interaction and pore-filling. Utilizing these results in our research indicates that the electrostatic interaction was not involved in the adsorption mechanism of NOR adsorption by GO with the presence of TA. The main adsorption interactions were the combination between  $\pi$ - $\pi$  EDA interaction, hydrogen bonding and hydrophobic interaction between NOR molecule and GO. Finally, a selective mechanism for the NOR adsorption by GO under the presence of TA could be proposed as illustrated in Fig. 6.

### 3.6. Comparison of adsorption capacity of NOR onto GO with other adsorbents

To determine the effectiveness of GO as adsorption selectivity, the adsorption capacity of GO under the presence of TA as coexisting natural matter (NOM) was compared with other adsorbents as presented in Table 7. To the best of our knowledge, there was a limit to the adsorption of NOR under the presence of NOM. Among the prior studies, this synthesized GO has the highest adsorption capacity of NOR under the

presence of NOM. It was reported that the adsorption capacity of NOR was suppressed under the presence of humic acid onto other adsorbents [4,49]. In contrast to the others, the adsorption capacity of NOR onto modified graphene oxide (P-GO) was enhanced by coexisting humic acid [41]. These results imply that this synthesized GO exhibited the selective properties for the removal of NOR in the adsorption process.

## 4. Conclusions

From the adsorption study of NOR by GO at different pH (pH 5, 7 and 9), equilibrium data were obtained and they were fitted to three nonlinear Langmuir, Freundlich and Sips adsorption isotherm models. The data were well fitted by Sips isotherm model that indicated the adsorption mechanism of NOR onto GO could be described as a combination of the Langmuir and Freundlich isotherm models. When the maximum adsorption capacity of NOR onto GO by Sips isotherm model was consistent with the experimental value that was found to be 124.18 mg g<sup>-1</sup> at pH 5 that higher than the other one (pH 7–9). Also the optimization of NOR's adsorption by the GO under the presence of TA was evaluated via BBD combined with RSM. The results showed that the initial concentration of NOR was the most significant factor when it came to its adsorption capacity. While the presence of TA insignificantly affected the adsorption capacity of NOR by the adsorbents in various pH conditions. Even the surface charge of the adsorbent and chemical structure of NOR directly affected by the pH value of the solution. These results imply that the electrostatic interaction was not involved in the adsorption interaction. Thereby, the peak adsorption capacity was reached when the pH level ranged from 6 to 9; the zwitterionic form of NOR was the main dominant, implying the hydrophobic interaction was involved during the adsorption process. However,  $\pi$ - $\pi$

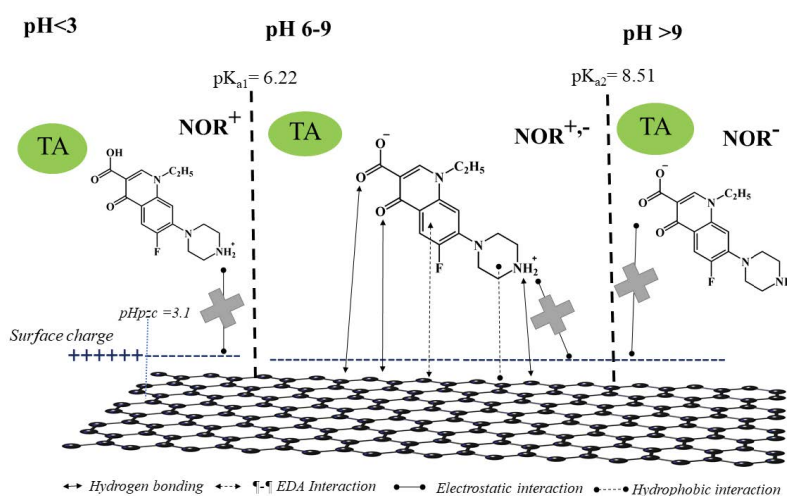


Fig. 6. Proposed mechanism of the adsorption of NOR by GO under the presence of TA.

Table 7

Comparison of adsorption capacity for NOR adsorption onto GO under the presence of natural organic matter (NOM) with other adsorbents

Adsorbents	NOM	Concentration of NOM (mg/L)	$q_e$ (mg/g)	Reference
Biochar	Humic acid	20	6	[4]
Montmorillonite-biochar	Humic acid	20	15	[4]
Titanium oxide	Humic acid	50	11	[49]
Modified graphene oxide (P-GO)	Humic acid	16	110	[41]
Powder activated carbon	Tannic acid	25	80	This work
Graphene oxide	Tannic acid	25	128	This work

EDA interaction and hydrogen bonding between NOR molecules and the functional group/physicochemical properties of GO was revealed through XPS analysis. Therefore, the combination of  $\pi$ - $\pi$  EDA interaction, hydrogen bonding and hydrophobic interaction was revealed as the main adsorption mechanism of NOR under the presence of TA.

### Acknowledgments

This research was funded by the Thailand Research Fund (TRF) (Contract no. MRG6080166). This work was carried out in the framework of the research program in “Hazardous Substance Management in Agricultural Industry” granted by the Center of Excellence on Hazardous Substance Management (HSM). The authors would like to express their gratitude to the Faculty of Science, Energy and Environment, King Mongkut’s University of Technology North Bangkok (Rayong Campus) for providing the necessary equipment.

### Supplementary data

Supplementary data consist of the physicochemical properties of GO and PAC, their adsorption behavior as adsorption kinetics, the effect of adsorbent dosage and pH over adsorption capacities of NOR.

### References

- [1] Y. Ben, H.F. Caixia, L. Min, W. Lei, H. Ming, C. Zheng, Human health risk assessment of antibiotic resistance associated with antibiotic residues in the environment: a review, *Environ. Res.*, 169 (2019) 483–493.
- [2] V. Homem, L. Santos, Degradation and removal methods of antibiotics from aqueous matrices: a review, *J. Environ. Manage.*, 92 (2011) 2304–2347.
- [3] A. Jia, Y. Wan, Y. Xiao, J. Hu, Occurrence and fate of quinolone and fluoroquinolone antibiotics in a municipal sewage treatment plant, *Water Res.*, 46 (2012) 387–394.
- [4] J. Zhang, M. Lu, J. Wan, Y. Sun, H. Lan, X. Deng, Effects of pH, dissolved humic acid and  $\text{Cu}^{2+}$  on the adsorption of norfloxacin on montmorillonite-biochar composite derived from wheat straw, *Biochem. Eng. J.*, 130 (2018) 104–112.
- [5] Y. Xiang, Z. Xu, Y. Wei, Y. Zhou, X. Yang, Y. Yang, J. Yang, J. Zhang, L. Luo, Z. Zhou, Carbon-based materials as adsorbent for antibiotics removal: mechanisms and influencing factors, *J. Environ. Manage.*, 237 (2019) 128–138.
- [6] F.F. Liu, J. Zhao, S. Wang, B. Xing, Adsorption of sulfonamides on reduced graphene oxides as affected by pH and dissolved organic matter, *Environ. Pollut.*, 210 (2016) 85–93.
- [7] F. Lian, B. Sun, X. Chen, L. Zhu, Z. Liu, B. Xing, Effect of humic acid (HA) on sulfonamide sorption by biochars, *Environ. Pollut.*, 204 (2015) 306–312.
- [8] X. Qin, P. Du, J. Chen, F. Liu, G. Wang, L. Weng, Effects of natural organic matter with different properties on levofloxacin adsorption to goethite: experiments and modeling, *Chem. Eng. J.*, 345 (2018) 425–431.
- [9] P. Prarat, P. Hongsawat, P. Punyapalaku, Amino-functionalized mesoporous silica-magnetic graphene oxide nanocomposites as water-dispersible adsorbents for the removal of the oxytetracycline antibiotic from aqueous solutions: adsorption performance, effects of coexisting ions, and natural organic matter, *Environ. Sci. Pollut. Res. Int.*, 27 (2020) 6560–6576.
- [10] G. Ersan, G.A. Onur, F. Perreault, T. Karanfil, Adsorption of organic contaminants by graphene nanosheets: a review, *Water Res.*, 126 (2017) 385–398.
- [11] H. Rasoulzadeh, A.M. Bandpei, M. Hosseini, M. Safari, Mechanistic investigation of ciprofloxacin recovery by magnetite-imprinted chitosan nanocomposite: isotherm, kinetic, thermodynamic and reusability studies, *Int. J. Biol. Macromol.*, 133 (2019) 712–721.
- [12] Y. Sun, Y. Yang, M. Yang, F. Yu, J. Ma, Response surface methodological evaluation and optimization for adsorption removal of ciprofloxacin onto graphene hydrogel, *J. Mol. Liq.*, 284 (2019) 124–130.
- [13] S. Karimifard, M.R.A. Moghaddam, Application of response surface methodology in physicochemical removal of dyes from wastewater: a critical review, *Sci. Total Environ.*, 640–641 (2018) 772–797.
- [14] B. Zhang, X. Han, P. Gu, S. Fang, J. Bai, Response surface methodology approach for optimization of ciprofloxacin adsorption using activated carbon derived from the residue of desilicated rice husk, *J. Mol. Liq.*, 238 (2017) 316–325.
- [15] M.A. Bezerra, R.E. Santelli, E.P. Oliveira, L.S. Villar, L.A. Escalera, Response surface methodology (RSM) as a tool for optimization in analytical chemistry, *Talanta*, 76 (2008) 965–977.
- [16] B. Yan, C.H. Niu, Adsorption behavior of norfloxacin and site energy distribution based on the Dubinin-Astakhov isotherm, *Sci. Total Environ.*, 631–632 (2018) 1525–1533.
- [17] H. Ghous, B. Haddou, M. Kameche, J.P. Canselier, C. Gourdon, Removal of tannic acid from aqueous solution by cloud point extraction and investigation of surfactant regeneration by microemulsion extraction, *J. Surfactants Deterg.*, 19 (2016) 57–66.
- [18] N. Yadav, B. Lochab, A comparative study of graphene oxide: Hummers, intermediate and improved method, *FlatChem*, 13 (2019) 40–49.
- [19] M. Aazza, H. Ahlafi, H. Moussout, H. Maghat, Ortho-nitrophenol adsorption onto alumina and surfactant modified alumina: kinetic, isotherm and mechanism, *J. Environ. Chem. Eng.*, 5 (2017) 3418–3428.
- [20] A. Gunay, E. Arslankaya, I. Tosun, Lead removal from aqueous solution by natural and pretreated clinoptilolite: adsorption equilibrium and kinetics, *J. Hazard. Mater.*, 146 (2007) 362–371.

- [21] Z. Zhang, H.C. Schniepp, D.H. Adamson, Characterization of graphene oxide: variations in reported approaches, *Carbon*, 154 (2019) 510–521.
- [22] S. Sakulpaisan, T. Vongsetskul, S. Reamouppaturm, J. Luangkachao, J. Tantirungrotechai, P. Tangboriboonrat, Titania-functionalized graphene oxide for an efficient adsorptive removal of phosphate ions, *J. Environ. Manage.*, 167 (2016) 99–104.
- [23] N. Ninwiwek, P. Hongswat, P. Punyapalaku, P. Prarat, Removal of the antibiotic sulfamethoxazole from environmental water by mesoporous silica-magnetic graphene oxide nanocomposite technology: adsorption characteristics, coadsorption and uptake mechanism, *Colloids Surf. A*, 580 (2019) 123716.
- [24] M. Acik, G. Lee, C. Mattevi, M. Chhowalla, K. Cho, Y.J. Chabal, The unusual infrared-absorption mechanism in thermally reduced graphene oxide, *Nat. Mater.*, 9 (2010) 840–845.
- [25] J. Shen, G. Huang, C. An, X. Xin, C. Huang, S. Rosendahl, Removal of tetrabromobisphenol A by adsorption on pinecone-derived activated charcoals: Synchrotron FTIR, kinetics and surface functionality analyses, *Bioresour. Technol.*, 247 (2018) 812–820.
- [26] K.Y. Foo, B.H. Hameed, Insights into the modeling of adsorption isotherm systems, *Chem. Eng. J.*, 156 (2010) 2–10.
- [27] S.A. Thayyath, D. Peethambaran, N. Jayachandran, Utilization of polypyrrole coated iron-doped titania based hydrogel for the removal of tetracycline hydrochloride from aqueous solutions: adsorption and photocatalytic degradation studies, *Environ. Nanotechnol. Monit. Manage.*, 4 (2015) 106–117.
- [28] A.B. Perez-Marin, V.M. Zapata, J.F. Ortuno, M. Aguilar, J. Saez, M. Llorens, Removal of cadmium from aqueous solutions by adsorption onto orange waste, *J. Hazard. Mater.*, 139 (2007) 122–131.
- [29] Y. Keren, M. Borisover, N. Bukhanovsky, Sorption interactions of organic compounds with soils affected by agricultural olive mill wastewater, *Chemosphere*, 138 (2015) 462–468.
- [30] L. Fang, Y. Miao, D. Wei, Y. Zhang, Y. Zhou, Efficient removal of norfloxacin in water using magnetic molecularly imprinted polymer, *Chemosphere*, 262 (2021) 128032.
- [31] X. Fang, S. Wu, Y. Wu, W. Yang, Y. Li, J. He, P. Hong, M. Nie, C. Xie, Z. Wu, K. Zhang, L. Kong, J. Liu, High-efficiency adsorption of norfloxacin using octahedral UiO-66-NH<sub>2</sub> nanomaterials: dynamics, thermodynamics, and mechanisms, *Appl. Surf. Sci.*, 518 (2020) 146226.
- [32] G. Peng, M. Zhang, S. Deng, D. Shan, Q. He, G. Yu, Adsorption and catalytic oxidation of pharmaceuticals by nitrogen-doped reduced graphene oxide/Fe<sub>3</sub>O<sub>4</sub> nanocomposite, *Chem. Eng. J.*, 341 (2018) 361–370.
- [33] X. Zhang, J. Shen, N. Zhuo, Z. Tian, P. Xu, Z. Yang, W. Yang, Interactions between antibiotics and graphene-based materials in water: a comparative experimental and theoretical investigation, *ACS Appl. Mater. Interfaces*, 8 (2016) 24273–24280.
- [34] H. Rasoulzadeh, M.H. Dehghani, Rasoulzadeh, A.S. Mohammadi, R.R. Karri, R. Nabizadeh, S. Nazmara, K.H. Kim, J.N. Sahu, Parametric modelling of Pb(II) adsorption onto chitosan-coated Fe<sub>3</sub>O<sub>4</sub> particles through RSM and DE hybrid evolutionary optimization framework, *J. Mol. Liq.*, 297 (2020) 111893.
- [35] H. Soleimanzadeh, A. Niaei, D. Salari, A. Tarjomannejad, S. Penner, M. Grünbacher, S.A. Hosseini, M.S. Mousavi, Modeling and optimization of V<sub>2</sub>O<sub>5</sub>/TiO<sub>2</sub> nanocatalysts for NH<sub>3</sub>-Selective catalytic reduction (SCR) of NO<sub>x</sub> by RSM and ANN techniques, *J. Environ. Manage.*, 238 (2019) 360–367.
- [36] J.F. Hair, G.T.M. Hult, C.M. Ringle, M. Sarstedt, *A Primer on Partial Least Squares Structural Equation Modeling (PLS-SEM)*, Sage, Thousand Oaks, 2017, p. 224.
- [37] I. Levchuk, J.J. Rueda Marquez, M. Sillanpaa, Removal of natural organic matter (NOM) from water by ion exchange: a review, *Chemosphere*, 192 (2018) 90–104.
- [38] W. Yang, Y. Lu, F. Zheng, X. Xue, N. Li, D. Liu, Adsorption behavior and mechanisms of norfloxacin onto porous resins and carbon nanotube, *Chem. Eng. J.*, 179 (2012) 112–118.
- [39] X. Wang, R. Yin, L. Zeng, M. Zhu, A review of graphene-based nanomaterials for removal of antibiotics from aqueous environments, *Environ. Pollut.*, 253 (2019) 100–110.
- [40] K. Sun, S. Dong, Y. Sun, B. Gao, W. Du, H. Xu, J. Wu, Graphene oxide-facilitated transport of levofloxacin and ciprofloxacin in saturated and unsaturated porous media, *J. Hazard. Mater.*, 348 (2018) 92–99.
- [41] N. Yao, X. Zhang, Z. Yang, W. Yang, Z. Tian, L. Zhang, Norfloxacin and Bisphenol-A removal using temperature-switchable graphene oxide, *ACS Appl. Mater. Interfaces*, 10 (2018) 29083–29091.
- [42] Z. Wang, X. Yu, B. Pan, B. Xing, Norfloxacin sorption and its thermodynamics on surface-modified carbon nanotubes, *Environ. Sci. Technol.*, 44 (2010) 978–984.
- [43] Y. Tang, H. Guo, L. Xiao, S. Yu, N. Gao, Y. Wang, Synthesis of reduced graphene oxide/magnetite composites and investigation of their adsorption performance of fluoroquinolone antibiotics, *Colloid Surf. A*, 424 (2013) 74–80.
- [44] W. Konicki, M. Aleksandrak, D. Moszynski, E. Mijowska, Adsorption of anionic azo-dyes from aqueous solutions onto graphene oxide: equilibrium, kinetic and thermodynamic studies, *J. Colloid Interface Sci.*, 496 (2017) 188–200.
- [45] X. Wu, M. Huang, T. Zhou, J. Mao, Recognizing removal of norfloxacin by novel magnetic molecular imprinted chitosan/ $\gamma$ -Fe<sub>2</sub>O<sub>3</sub> composites: selective adsorption mechanisms, practical application and regeneration, *Sep. Purif. Technol.*, 165 (2016) 92–100.
- [46] R. Rostamian, H. Behnejad, A comprehensive adsorption study and modeling of antibiotics as a pharmaceutical waste by graphene oxide nanosheets, *Ecotoxicol. Environ. Saf.*, 147 (2018) 117–123.
- [47] S. Dong, Y. Sun, J. Wu, B. Wu, A.E. Creamer, B. Gao, Graphene oxide as filter media to remove levofloxacin and lead from aqueous solution, *Chemosphere*, 150 (2016) 759–764.
- [48] H. Chen, G. Bin, L. Hui, Removal of sulfamethoxazole and ciprofloxacin from aqueous solutions by graphene oxide, *J. Hazard. Mater.*, 282 (2015) 201–207.
- [49] H. Peng, S. Feng, X. Zhang, Y. Li, X. Zhang, Adsorption of norfloxacin onto titanium oxide: effect of drug carrier and dissolved humic acid, *Sci. Total Environ.*, 438 (2012) 66–71.

## Supplementary information

Table S1  
Physicochemical properties of carbonaceous adsorbents

Adsorbent	Pore size (nm)	Surface area (m <sup>2</sup> /g)	Pore volume (cm <sup>3</sup> /g)	pH <sub>pzc</sub>	Element composition		
					C %	O %	H %
PAC	2.04	947.84	0.69	7.10	71.03	25.63	3.34
GO	2.83	192.76	0.14	3.10	45.26	2.74	52.00

Table S2  
Adsorption isotherm of NOR onto PAC constants and statistical comparison values

Isotherm	pH		
	5	7	9
<b>Langmuir</b>			
$q_m$ (mg g <sup>-1</sup> )	101.94	313.91	71.47
$B$	0.0347	0.0119	0.0256
$R^2$	0.9961	0.9954	0.9861
Chi square	0.17	0.87	0.4414
<b>Freundlich</b>			
$K_f$ (mg g <sup>-1</sup> )	13.77	9.50	5.37
$1/n$	0.3807	0.6322	0.4995
$R^2$	0.9598	0.9775	0.9522
Chi square	1.60	0.12	1.42
<b>Sips</b>			
$q_m$ (mg g <sup>-1</sup> )	92.47	229.21	61.14
$B$	0.0208	0.0064	0.0198
$1/n$	1.2215	1.3172	1.17
$R^2$	0.9985	0.9957	0.9937
Chi square	0.04	0.11	0.314

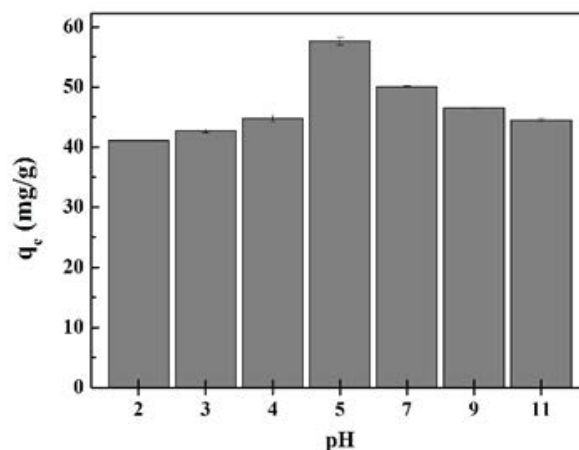


Fig. S2. Effect of solution pH on the adsorption of NOR onto GO.

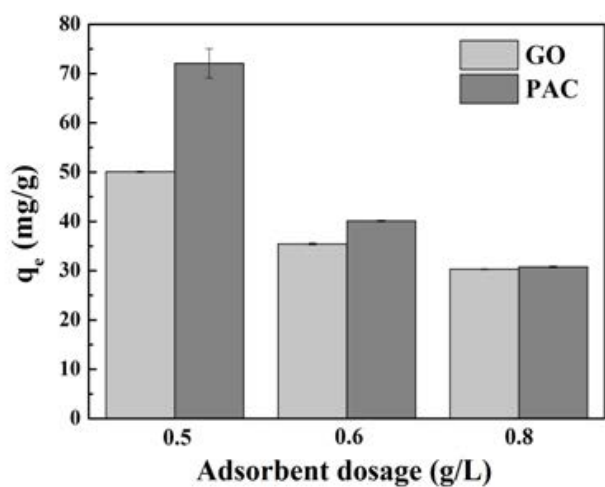


Fig. S1. Effect of dosage on adsorption capacity of NOR onto GO and PAC.